Virtual Crack Closure Technique Based on MSIM Method

Feng Su [1, 2], Jie Wu [1, 2, *], Yongchang Cai [1, 2]

[1] State Key Laboratory for disaster reduction in Civil Engineering, Tongji University, Shanghai, China 200092;
[2] Key Laboratory of Geotechnical and Underground Engineering of Ministry of Education, Tongji University, Shanghai, China 200092;
* Corresponding author: jiee.wu@gmail.com

Abstract The virtual crack closure technique is applied to the calculation of stress intensity factor (SIF) in the framework of meshless Shepard interpolation method (MSIM). In the MSIM interpolation, the Shepard shape functions are used for the partition of unity and the local cover functions are separately constructed for the nodes on the boundary and inside the domain. There are three desirable properties in the MSIM including the completeness property, the delta property which lead to easy boundary treat and the low computational expense of the shape function. In the virtual crack closure technique, the assistant finite element mesh is added beside the crack tips, and the SIFs are calculated naturally and effectively near the tips by using the MSIM. Numerical result for a star-shaped crack in a square plate is reported to demonstrate the correctness and robust of the present method.

Keywords Meshless Shepard interpolation method, Partition of unity method, Virtual crack closure technique, Stress intensity factor

1. Introduction

Calculating of parameters such as stress intensity factor, J integral and strain energy release rate are always highly important but not well addressed in fracture mechanics, and lots of efforts have been devoted by the researchers and engineers in recent years. Analytic solutions for some particular structural components have been proposed and expressed as functions, line graft or tables, which can be referred in some handbooks compiled for the engineers [1-3]. However, the limited number of analytic solutions is far from the satisfaction of the need in the real world. The numerical calculations for the parameters in fracture mechanics become necessary in term of the realistic when considering the dramatically development of the hardware and software of computers [4-9].

J integral was proposed by Rice in 1969 and was introduced into the element free Galerkin method by Brighenti [7]. This method is attractive for the calculation of SIF because of its completeness of theory, high accuracy and path-independent integration. But the inappropriate determination of the radius of the integration circle may degrade the accuracy of J integral when dealing with problems involving short crack segment such as broken cracks and crack tips near the boundaries.

Virtual crack closure technique (VCCT) requires only 2 parameters (the nodal force and displacement near the crack tip) which can be obtained naturally in the FEM method to evaluate the SIF and, besides, the calculation results are often reliable and not effected by the small length of crack tips. Consequently, it is paid increasingly more attention by the researchers. However, at present, the VCCT is always carried out in the framework of the FEM, which is unavoidably encountered with the mesh refinement. More details about VCCT can refer to [10].

To alleviate this drawback, the meshless Shepard interpolation method (MSIM) [11] is used to model the discontinuous stress field near the crack and stress singularity near the crack tips and then, the stress and displacement results are used by the VCCT to evaluate the SIF. The time consuming remeshing process is unnecessary in this method and makes the simulation much more reliable and possessing high accuracy. Details of meshless simulation of discontinuous model and the determination of the SIF are provided. In the end, the method described here is used to analyze a square plate with a star-shape crack. The results obtained by the present method are compared with

reference solutions available showing the implementation effectively to model the discontinuous and to evaluate the SIF.

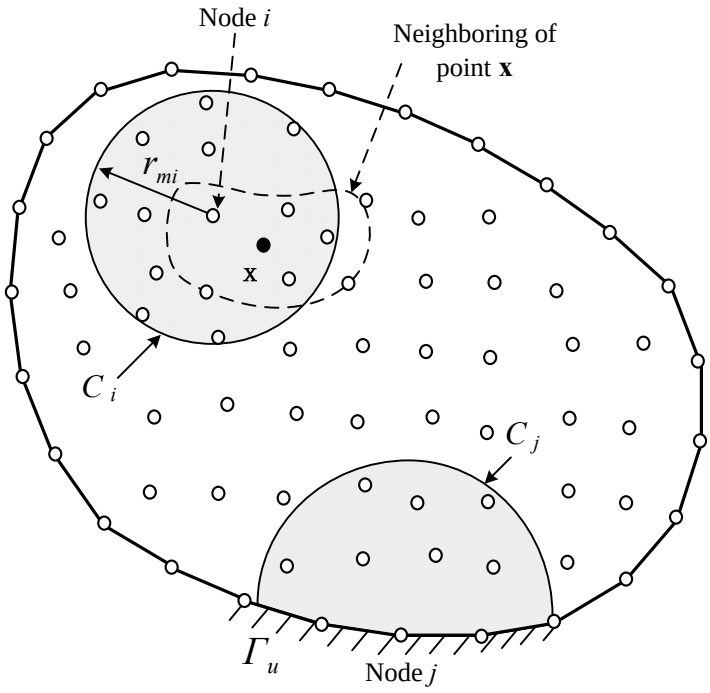

Figure 1. Discrete model of domain Ω

2. The PU-based meshless Shepard interpolation

Consider a two-dimensional domain Ω, and let Ω be discretized by N scattered nodes as shown in Fig. 1. For each node i, a circle cover (subdomain)

$$C_i = \{\mathbf{x} \in \Omega : \|\mathbf{x} - \mathbf{x}_i\| \le r_{mi}\}, \tag{1}$$

is attached. Here, r_{mi} is the radius of the cover C_i. The displacements associated with the node i are denoted by (u_{i0}, v_{i0}).

For a given point X($X \in \Omega$), based on the PU concept, a new interpolation $u^h(X)$ at X can be defined by

$$u^h(X) = \sum_{i-1}^{n} \emptyset_i^0(x)\, u_i^i(X) \tag{2}$$

where n is the total number of neighboring nodes where the position of point $\mathbf{X}$ located in the cover support. $u_i^l(\mathbf{x})$ are the cover interpolations defined on the cover of node i.

In MSIM, the interpolations are constructed separately for the nodes on the essential boundary or in the domain.. $\phi_i^0(\mathbf{x})$ is the Shepard function or zeroth-order function

$$\phi_i^0(\mathbf{x}) = \frac{w_i(\mathbf{x})}{\sum_{i=1}^{n} w_i(\mathbf{x})} \tag{3}$$

where $w_i(\mathbf{x})$ is the weight function associated with node i.

The Shepard function $\phi_i^0(\mathbf{x})$ in Eq. (3) satisfies the delta property if weight function is singular at $\mathbf{x} = \mathbf{x}_i$. The weight function[12] adopted here is

$$w_i(\mathbf{x})=\begin{cases}\dfrac{d_{mi}^2}{d_i^2+\varepsilon}\cos^2\left(\dfrac{\pi d_i}{2d_{mi}}\right), & d_i \le d_{mi}\\ 0 & d_i > d_{mi}\end{cases} \tag{4}$$

where $d_i=\|\mathbf{x}-\mathbf{x}_i\|$ is the Euclidian distance between the point $\mathbf{x}$ and node $\mathbf{x}_i$, and ε is a small number to avoid the numerical difficulty resulting from the singularity at nodes.

On each cover C_i, a local approximation is first expressed as

$$u_i^l(\mathbf{x}) = \mathbf{P}^{\mathrm{T}}(\mathbf{x})\mathbf{a}(\mathbf{x}) = \sum_{k=1}^{m} p_k(\mathbf{x})a_k \tag{5}$$

where m is the number of terms in the basis, $\mathbf{p}^{\mathrm{T}}(\mathbf{x})=[1,x,y,xy.....]$ are the nominal basis functions, a_i is their coefficients. Here, the bilinear basis $\mathbf{p}^{\mathrm{T}}(\mathbf{x})=[1,x,y,xy]$ is used as an example to introduce the construction of the MSIM interpolation.

2.1 Cover interpolation for the nodes not located on the essential boundary

For the typical node i not located on the essential boundary, the local cover approximation is directly taken as

$$u_i^l(\mathbf{x}) = u_i^{\ln}(\mathbf{x}) = a_{1i} + a_{2i}x + a_{3i}y + a_{4i}xy \tag{6}$$

Let the cover function at the node i satisfy the condition

$$u_i^{\ln}(x_i) = a_{1i} + a_{2i}x_i + a_{3i}y_i + a_{4i}x_iy_i = u_{i0} \tag{7}$$

Hence,

$$a_{1i} = u_{i0} - a_{2i}x_i - a_{3i}y_i - a_{4i}x_iy_i \tag{8}$$

Substituting Eq. (8) into Eq. (3) leads to

$$u_i^{\ln}(\mathbf{x})=u_{i0}+a_{2i}(x-x_i)+a_{3i}(y-y_i)+a_{4i}(xy-x_iy_i) = \overline{\mathbf{\Psi}}^i\mathbf{T}_x^i \tag{9}$$

where

$$\overline{\mathbf{\Psi}}^i(\mathbf{x})=[\Psi_1^i \quad \Psi_2^i \quad \Psi_3^i \quad \Psi_4^i]=[1 \quad x-x_i \quad y-y_i \quad xy-x_iy_i] \tag{10}$$

$$\mathbf{T}_x^i=[u_{i0} \quad a_{2i} \quad a_{3i} \quad a_{4i}]^T \tag{11}$$

Similarly, the y-displacement interpolation $v_i^{\ln}(x_i)$ is given by

$$v_i^{\ln}(\mathbf{x})=v_{i0}+b_{2i}(x-x_i)+b_{3i}(y-y_i)+b_{4i}(xy-x_iy_i) = \overline{\mathbf{\Psi}}^i\mathbf{T}_y^i \tag{12}$$

where

$$\mathbf{T}_y^i=[v_{i0} \quad b_{2i} \quad b_{3i} \quad b_{4i}]^T \tag{13}$$

Eq. (9) and (12) can be rewritten in the form

$$\mathbf{u}_i^{\ln}(\mathbf{x})=\begin{Bmatrix}u_i^{\ln}(\mathbf{x})\\ v_i^{\ln}(\mathbf{x})\end{Bmatrix}=\mathbf{\Psi}^i\mathbf{T}^i \tag{14}$$

where

$$\mathbf{\Psi}=\begin{bmatrix}1 & 0 & x-x_i & 0 & y-y_i & 0 & xy-x_iy_i & 0\\ 0 & 1 & 0 & x-x_i & 0 & y-y_i & 0 & xy-x_iy_i\end{bmatrix} \tag{15}$$

$$\mathbf{T}=[u_{i0} \quad v_{i0} \quad a_{2i} \quad b_{2i} \quad a_{3i} \quad b_{3i} \quad a_{4i} \quad b_{4i}]^T \tag{16}$$

(u_{i0},v_{i0}) are the nodal displacement of node i, $(a_{2i},b_{2i},a_{3i},b_{3i},a_{4i},b_{4i})$ are the extra freedoms of cover C_i. From Eq. (14), we observe that

$$\mathbf{u}_i^{\ln}(x_i, y_i) = \begin{Bmatrix} u_{i0} \\ v_{i0} \end{Bmatrix} \tag{17}$$

It means that the cover function of the node i is interpolated in terms of nodal displacements (u_{i0}, v_{i0}).

2.2 Cover interpolation for the nodes located on the essential boundary

For a typical node j located on the essential boundary, suppose that there M nodes in the support of cover C_j (Fig. 1). At the local cover C_j, a discrete error norm is defined as

$$u_j^{lb}(\mathbf{x}) = \overline{\mathbf{\Phi}}^j(\mathbf{x})\mathbf{u}_0^j = \sum_{k=1}^{M} \overline{\Phi}_k^j(\mathbf{x}) u_k \tag{18}$$

where

$$\overline{\mathbf{\Phi}}^j(\mathbf{x}) = [\Phi_1^j(\mathbf{x}) - \Phi_1^j(\mathbf{x}_j), \ \cdots, \ 1 + \Phi_j^j(\mathbf{x}) - \Phi_j^j(\mathbf{x}_j), \ \cdots, \ \Phi_M^j(\mathbf{x}) - \Phi_M^j(\mathbf{x}_j)] \tag{19}$$

x_j is the coordinate of node j.

Similarly, the y-displacement interpolation $v_j^{lb}(\mathbf{x})$ is given by

$$v_j^{lb}(\mathbf{x}) = \mathbf{\Phi}^j(\mathbf{x})\mathbf{V}_0^{\ j} = \sum_{k=1}^{M} \Phi_k^j(\mathbf{x}) v_k \tag{20}$$

where

$$\mathbf{V}_0^j = \begin{bmatrix} v_{10} & v_{20} & \cdots & v_{M0} \end{bmatrix} \tag{21}$$

Eq. (18) and (20) can be rewritten in the form

$$\mathbf{u}_j^{lb}(\mathbf{x}) = \begin{Bmatrix} u_j^{lb}(\mathbf{x}) \\ v_j^{lb}(\mathbf{x}) \end{Bmatrix} = \mathbf{\Phi}_*^j \mathbf{D}^j \tag{22}$$

where

$$\mathbf{\Phi}_*^j = \begin{bmatrix} \overline{\Phi}_1^j & 0 & \cdots & \overline{\Phi}_M^j & 0 \\ 0 & \overline{\Phi}_1^j & \cdots & 0 & \overline{\Phi}_M^j \end{bmatrix} \tag{23}$$

$$\mathbf{D}^j = \begin{bmatrix} u_{10} & u_{10} & u_{20} & u_{20} & \cdots & \cdots & u_{M0} & u_{M0} \end{bmatrix} \tag{24}$$

Substituting Eq. (14) and (22) into Eq. (2) leads to

$$u^h(\mathbf{x}) = \sum_{i=1}^{n} \phi_i^0(\mathbf{x}) u_i^l(\mathbf{x}) = \sum_{i=1}^{n_1} \phi_i^0(\mathbf{x}) u_i^{\ln}(\mathbf{x}) + \sum_{j=1}^{n_2} \phi_j^0(\mathbf{x}) \left(\sum_{k=1}^{M} \overline{\Phi}_k^j(\mathbf{x}) u_k \right) \tag{25}$$

where $n = n_1 + n_2$ is the total number of neighboring nodes where the position point $\mathbf{x}$ located in the cover support, n_1 denotes the node set not on the essential boundary, n_2 denotes the node set located on the essential boundary. The MSIM possesses the delta property and preserves the completeness of the field up to the order of the basis. The proof of these properties can be referred to [11].

3. The application of virtual crack closure technique in MSIM

Virtual crack closure technique (VCCT) is proposed by Rybicki and Kanninen [10] mainly dealing with two dimensional problems. In this method, the strain energy release rate for the crack propagation is always calculated based on the FEM analysis results. Here, taking a finite crack body as an example, the basic concept of virtual crack closure technique will be briefly introduced.

The length of crack is a, and the propagation length is Δa. When the quadrangle mesh is employed,

the stain energy release rate of the crack could be calculated by

$$G_I \cong \frac{F_{y1}\Delta v_{3,4}}{2B\Delta a} \tag{26a}$$

$$G_{II} \cong \frac{F_{x1}\Delta u_{3,4}}{2B\Delta a} \tag{26b}$$

where, F_{x1} and F_{y1} are the node forces (X direction, Y direction, respectively) belonging to node 1. $\Delta v_{3,4}$ and $\Delta u_{3,4}$ are the Y direction displacement and X direction displacement between node 3 and 4, respectively.

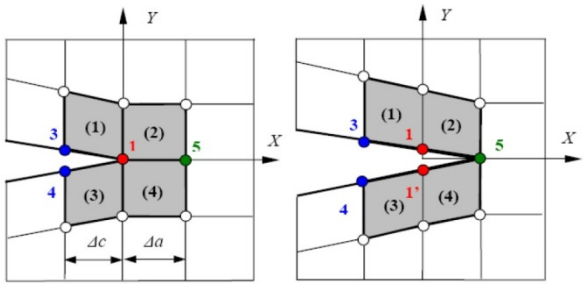

Figure 2. Illustration of calculating the strain energy release rate by the VCCT

Due to the fact that the virtual crack closure technique is always implemented in the framework of FEM, the remeshing during the simulation of crack propagation are unavoidably encountered. To solve this problem, the virtual crack closure technique will be introduced into MSIM in this section. Both the advantages of the two methods will be maintained to make the evaluation of the SIFs much more efficient. The progress will be carried out mainly in the following steps:

1) Construction of meshless numerical model;
2) Calculation of the displacement of the nodes based on the MSIM;
3) Setting the assistant mesh near the crack tip in order to calculate the nodal force
4) Constructing the global stiffness matrix of the assistant mesh and calculating the displacement of the node in the assistant mesh based on the MSIM.
5) Getting the nodal force near the crack tip by $F_e = K_e a_e$, where F_e is the assistant nodal force, K_e is the global stiffness matrix of the assistant mesh, a_e is the displacement vector of the assistant nodes.

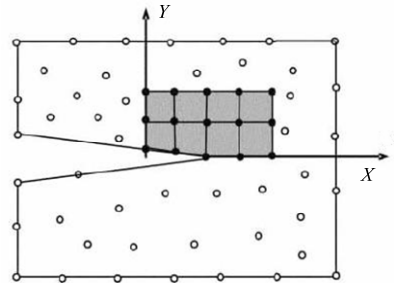

Figure 3. The assistant mesh employed in the MSIM to evaluate the nodal force

4. A case study on a finite plate with star-shaped crack

In this section, a star-shaped crack in a square plate subjected to bi-axial tension as shown in Fig.4 will be examined. The analysis is treated as plate strain problem, and the plate size is taken to be W = 2.0, and the bi-axial tension to be unity. The material constants are the Young's modulus

$E = 1 \times 10^7$ and the Poisson's ratio $\nu = 0.3$. The SIF of node A and B are calculated by both of the linear basis function and the enriched basis function with virtual crack closure technique. A meshless model is constructed as shown in Fig.5. The influence of crack geometry on the SIFs is also investigated by varying W/a (e.g.0.1W, 0.3W, 0.5W, 0.7W).

The normalized stress intensity factors at tips A and B are defined as $F_I^A = K_I^A / \sigma\sqrt{\pi a}$, $F_I^B = K_I^B / \sigma\sqrt{\pi a}$, $F_{II}^B = K_{II}^B / \sigma\sqrt{\pi a}$. The comparison between the calculation results and the reference solutions available [13] are demonstrated in Table 1. From this table, the excellent agreement of the computed SIF results and the reference solutions can be easily seen.

Table 1. Normalized SIFs comparison for a star-shaped crack

a/W	θ	*	MSIM(linear basis)	RE（%）	MSIM(enriched basis)	RE（%）
	F_I^A	0.751	0.736	-1.998	0.754	-0.533
0.1	F_I^B	0.769	0.758	-1.430	0.766	-0.391
	F_{II}^B	0.000	0.000	0.000	0.000	0.000
	F_I^A	0.793	0.778	-2.031	0.789	-0.504
0.3	F_I^B	0.798	0.786	-1.253	0.795	-0.376
	F_{II}^B	0.002	0.002	0.000	0.002	0.000
	F_I^A	0.886	0.868	-1.891	0.883	-0.456
0.5	F_I^B	0.926	0.912	-1.511	0.922	-0.432
	F_{II}^B	0.018	0.0176	-2.122	0.018	0.000
	F_I^A	1.097	1.084	-1.485	1.102	0.339
0.7	F_I^B	1.237	1.218	-1.536	1.233	-0.323
	F_{II}^B	0.059	0.058	-1.724	0.0586	-0.678

*Daux et al. (2000)

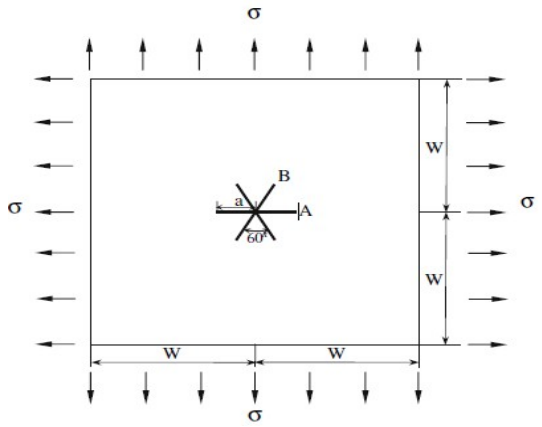

Figure 4. A star-shaped crack in a square plate under bi-axial tension

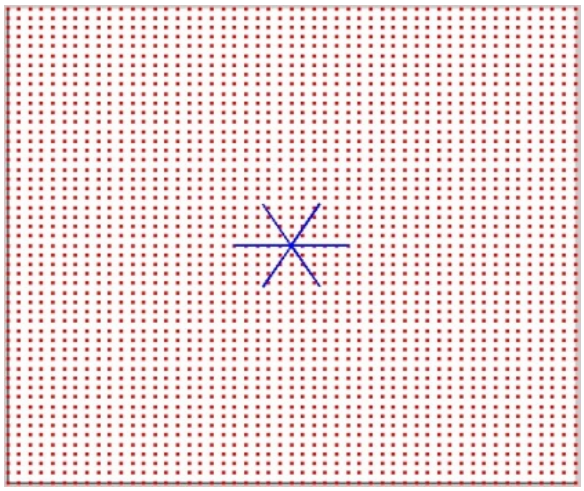

Figure 5. The meshless model of a star-shaped crack in a square plate

5. Conclusions

The application of virtual crack closure technique into the MSIM is presented in this paper. The remeshing and the refinement near the crack tips can be avoided in the present method, and as a result, it makes the evaluation of the SIF much easier and more efficient. The virtual crack closure technique is based on the stress analysis using the MSIM for discontinuous model here, however other meshless methods are equally viable, e.g., the element-free Galerkin method (EFG), and the meshless local-Petrov Galerkin method (MLPG). The numerical results indicate that the present method effectively calculates the SIF near the crack tips and possess a high accuracy.

Acknowledgements

The authors gratefully acknowledge the support of Program for New Century Excellent Talents (NCET-12-0415), the National Science and Technology Support Program (2011BAB08B01), and the Fundamental Research Funds for the Central Universities.

References

[1] Rooke D. P., Cartwright D.J. Compendium of stress intensityfactors[M]. London: Her Majesty’s Stationary Office, 1976
[2] Tada H., Paris P. C., Irwin G. R. The stress factor hand book [M]. Hellertown: Del Research Corporation, 1985
[3] Murakami Y. Stress intensity factors handbook[M]. New York: Pergamon, 1987
[4] Shahani A.R., Habibi S.E. Stress intensity factors in a hollow cylinder containing circumferential semi-elliptical crack sub-jected to combined loading[J]. International Journal of Fatigue, 2007, 29(1):128- 140
[5] Zhou W.Y., Xiao H.T.. Three dimension discontinuous displacement method and the strongly singular and hypersing ular integrals[J]. Acta Mechanica Sinica, 2002, 34(4): 645-651
[6] Citatella R., Perella M. Multiple surface crack propagation: numerical simulations and experimental tests[J]. Fatigue Fract Engng Mater Struct, 2005, 28(1/2): 135-148
[7] Brighenti R. Application of the element-free Galerkin meshless method to 3-D fracture mechanics problems[J]. Engineering Fracture Mechanics, 2005, 72(18):2808 - 2820
[8] Chihdar Y., Alireza C., Tomblin J.S. Strain energy release rate determination of prescribed cracks in adhesively-bonded single-lap composite joints with thick bondlines [J]. Composites: Part B, 2008, 39(5): 863 - 873.
[9] Rosa M., Freitas D.M. Characterisation of the edge crack torsion (ECT) test for the measurement of the mode III interlaminar fracture toughness[J]. Engineering Fracture Mechanics, 2009, 76(18): 2799 -2809.
[10] Rybicki E F, Kanninen M F. A finite element calculation of stress intensity factors by a modified crack closure integral. Engineering Fracture Mechanics, 1977, 9: 931-938
[11] Cai Y.C., Zhu H.H. A PU-based meshless Shepard interpolation method satisfying delta property [J].

Engineering Analysis with Boundary Elements, 2010, 34(1): 9-16.
[12] Lancaster P., Salkauskas K. Surfaces generated by moving least squares methods [J]. Mathematics of Computation, 1981, 37(2): 141-158
[13] Daux C., Moes N., Dolbow J., Sukumar N., Belytschko T. Arbitrary branched and intersecting cracks with the extended finite element method. Computer Methods in Applied Mechanics and Engineering, 2000, 48:1741- 1760.